SPANDIDOS PUBLICATIONS

Biomolecular diagnosis of human glioblastoma multiforme using Synchrotron mid-infrared spectromicroscopy

KAISER ALI[1], YANJIE LU[2], UMASHANKAR DAS[3], RAJENDRA K. SHARMA[4], SHELDON WIEBE[5], KOTOO MEGURO[6], VENKAT SADANAND[6], DARYL R. FOURNEY[6], ALEKSANDER VITALI[6], MICHAEL KELLY[6], TIM MAY[7], JOSE GOMEZ[8] and ERIC PELLERIN[9]

[1]Saskatoon Cancer Centre and University of Saskatchewan; [2]Cancer Research Unit, Saskatchewan Cancer Agency; [3]College of Pharmacy and Nutrition, University of Saskatchewan; [4]Deptartment of Pathology, University of Saskatchewan and Cancer Research Unit, Saskatchewan Cancer Agency; [5]Deptartment of Medical Imaging; [6]Division of Neurosurgery, University of Saskatchewan and Saskatoon Health Region; [7]Canadian Light Source; [8]Deptartment of Pathology, Saskatoon Health Region; [9]National Research Council, Winnipeg, Canada

Received February 2, 2010; Accepted March 5, 2010

DOI: 10.3892/ijmm_00000428

Abstract. Glioblastoma multiforme (GBM) is one of the most malignant human tumors, with a uniformly poor outcome. One obstacle in curing malignant brain tumors is the limitation of conventional light microscopy in detecting microscopic residual tumor in biopsy samples from the perimeter of the surgically resected tumor. We further refined the identification of GBM tumor tissue at the sub-cellular level, utilising the technique of Synchrotron, sourced mid-infrared (mid-IR) spectromicroscopy. Paired, thin (5 μm) cryosections of snap-frozen human GBM tumor samples removed at elective surgery were mounted on glass slides (hematoxylin and eosin-stained tissue section) and calcium fluoride (CaF_2) windows (unstained tissue section for transmission spectromicroscopy), respectively. Concordance of tumor bearing areas identified in the stained section with the unstained IR tissue section was confirmed by the pathologist of the study. Compared with molecular signatures obtained from normal control brain tissue, unique spectroscopic patterns were detected in GBM tumor samples from 6 patients. The identifying features of GBM were: i) high protein-to-lipid ratios (amide I+II/CH_2 symmetric stretch; amide I+II/CH_2+CH_3 symmetric and asymmetric stretch), and ii) considerable enhancement of the intensities of characteristic peaks at 2,957 and 2,871 cm^{-1} representing CH_3 asymmetric and symmetric stretch, respectively. Spectral data sets were subjected to Ward's algorithm for assignment to similar groups, and then subjected to hierarchical cluster analysis (HCA) by means of false color digital maps. False color images of 5 clusters obtained by HCA identified dominant clusters corresponding to tumor tissue. Corroboration of these findings in a larger number of GBM may allow for more precise identification of these and other types of brain tumors.

Correspondence to: Dr Kaiser Ali, Saskatoon Cancer Centre and University of Saskatchewan, 20 Campus Drive Saskatoon, SK S7N 4H4, Canada
E-mail: kaiser.ali@saskcancer.ca

Abbreviations: CaF_2, calcium fluoride; FTIR, Fourier Transform Infrared; GBM, glioblastoma multiforme; GFAP, glial fibrillary acid protein; H&E, hematoxylin and eosin; HCA, hierarchical cluster analysis; WHO, World Health Organisation

Key words: synchrotron, glioblastoma multiforme, mid-infrared spectromicroscopy, hierarchical cluster analysis

Introduction

Glioblastoma multiforme (GBM) is the most malignant brain tumor in humans, accounting for up to 45-50% of all gliomas in adults, and has a median survival time of 7.4 months (1). Curative management of human brain tumors is dependent upon accuracy of histological diagnosis and grading, achieving gross total surgical removal, and inclusion of residual macroscopic and microscopic tumor within radiation therapy fields (2). Time of progression of disease in patients undergoing tumor debulking surgery followed by radiation therapy and adjuvant single agent chemotherapy has been reported to be 6.7 months (3). Routine laboratory diagnosis of GBM currently consists of identification by light microscopy of pathognomonic histological and immunohistochemical staining patterns. The World Health Organisation (WHO) classification system categorises GBM as an astrocytic tumor with the highest grade of malignancy (Grade IV), based on the degrees on anaplasia and mitotic activity, as well as endothelial proliferation and/or necrosis (4,5). Recognition of histologic heterogeneity within brain tumors containing multiple phenotypes (6) are compelling reasons for developing more refined and accurate diagnostic techniques, which may help improve treatment outcomes.

Standard diagnosis of brain tumors is based on imaging and light microscopy examination of tissue sections stained with hematoxylin and eosin (H&E), and an array of immunohistochemical stains. Histological examination includes gradation of tumor cell density, vascularisation, small-cell

A B C

Figure 1. Paired, thin (5 μm) GBM tumor tissue sections (A and B). A, H&E stained section with superimposed digital boundaries (red lines) identifying perimeters of tumor-bearing areas. B, Corresponding unstained thin tumor section for IR spectroscopy. C, Spectromicroscopy-generated overview image of unstained tissue section with raster map (red rectangle) targeting area for IR spectroscopy.

Table I. Clinical summary of patients in Synchroton mid-IR study.

Case no.	Age (yrs)/sex	Diagnosis (WHO Classification - 2007)	Sample location
1	28/M	normal brain	R. temporal
2	11/M	normal brain	Suprasellar
3	59/M	Glioblastoma (9440/3)	L. temporo-pareital
4	69/M	Glioblastoma (9440/3)	R. occipital
5	50/F	Glioblastoma (9440/3)	L. occipital
6	47/M	Glioblastoma (9440/3)	Corpus callosum
7	61/F	Glioblastoma (9440/3)	R. frontal
8	51/M	Glioblastoma (9440/3)	R. frontal

density and matrix loosening, and the presence of necrosis, atypia, mitoses, and endothelial proliferation (7). GBM's are immunoreactive for glial fibrillary acid protein (GFAP), S-100, and have a high proliferative index as demonstrated by the Ki-67 marker (8). The epithelial monoclonal antibody marker, Ber-EP4, serves as a reliable negative control (9). However, GFAP reactivity can vary in GBM, and significant portions of this tumor may lack GFAP expression. Therefore, more refined and precise diagnostic tools are required.

Fourier Transform Infrared (FTIR) spectroscopy allows for qualitative and quantitative analysis of the basic components of biological tissues (lipids, proteins, carbohydrates and nucleic acids). The identifying spectra are recorded in the mid-infrared (mid-IR) light region between wave numbers 4,000-900 cm^{-1}, and analyzed for unique spectral 'signatures' (10-12). The technique of FTIR spectral mapping is quickly approaching its utility as a tool for molecular histopathology (13) by detection of subtle chemical changes in tumors indicative of tumor progression (14,15) and for identifying prognostic indicators (16). Conventional IR spectromicroscopy examination of biological tissues has limitations (17,18) including insufficient spatial resolution of only ~20-25 μm. These problems are overcome by Synchrotron IR light by virtue of its brightness, which is 100-1,000 times greater than that from a conventional source (19).

The objective was to determine whether a diagnostic molecular spectral 'signature' can be identified in human GBM tumor tissue samples by Synchrotron mid-IR spectromicroscopy.

Materials and methods

Ethics approval and informed consent. Prior approval for the research study was obtained from the University of Saskatchewan Biomedical Research Ethics Board. The responsible neurosurgeons obtained informed consent from their respective patients for tissue samples in advance of elective surgical resection at Royal University Hospital, Saskatoon.

Preparation of samples and acquisition of data. Tumor tissue was obtained from 6 patients with GBM and control samples from 2 patients (normal brain tissue from the margins of resected GBM tumor margins histologically confirmed by the pathologist of the study). Tissue sections were obtained and samples processed as previously described (20). Briefly, paired, thin (5 μm) brain tissue sections were cut in a cryostat at -20˚C. The first section was placed on a glass slide for H&E staining. The second unstained section was mounted onto a CaF_2 slide for mid-IR transmission spectromicroscopy at the 01B1-1 Beamline, Canadian Light Source, University of Saskatchewan campus. Concordance of tumor-bearing areas was achieved by superimposing a digital tractile grid over paired H&E and IR tissue section images, demarcating tumor-bearing areas within the tissue section, and then transferring onto the overview image generated by the spectromicroscope in preparation for mid-IR spectroscopy (Fig. 1).

Transmission spectromicroscopy was performed using an IFS 66v/S FTIR spectrometer with a Synchrotron mid-IR light source attached to a Hyperion IR microscope (Bruker

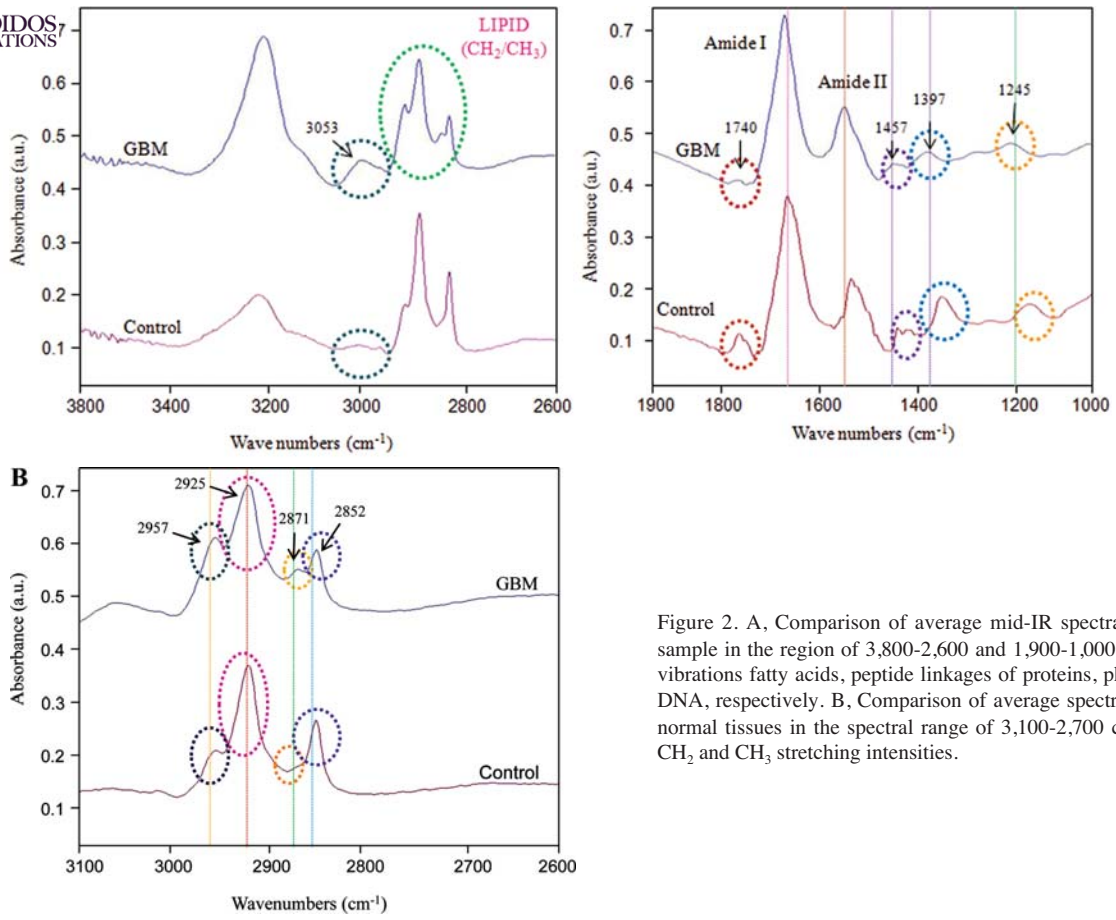

Figure 2. A, Comparison of average mid-IR spectra of GBM and control sample in the region of 3,800-2,600 and 1,900-1,000 cm^{-1} representing acyl vibrations fatty acids, peptide linkages of proteins, phosphodioxy groups of DNA, respectively. B, Comparison of average spectra of GBM tumour and normal tissues in the spectral range of 3,100-2,700 cm^{-1}, representing lipid CH_2 and CH_3 stretching intensities.

Optics Inc., Billerica, MA) with a 36X Cassegrain objective and a single channel MCT detector. Raster scans were obtained in the range of 4,000-900 cm^{-1} using a 10x10 micron aperture, 10 micron step size, 32 scans per step, and resolution of 4 cm^{-1}. Stage control, data collection and processing were done using OPUS (Bruker Optics) software. Visible images were obtained using a charged-couple device camera, linked to the infrared images. The resulting FTIR spectra were processed using Cytospec spectroscopic software (21). All FTIR spectra were uniformly subjected to base line correction using the Savitzky-Golay method and noise reduction to level 5. To generate peak ratios, peak areas of individual peaks were calculated using integration method C. A multivariate statistical analysis was performed after converting all spectra to their second derivative and subjecting them to hierarchical cluster analysis (HCA). Pseudo-color maps based on cluster analysis were then created by assigning a color to each spectral cluster.

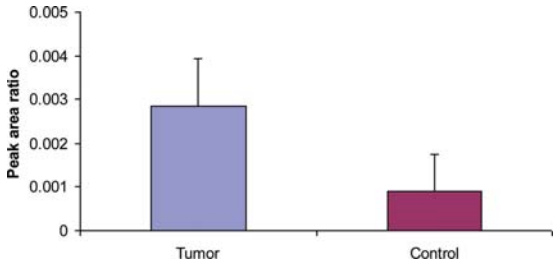

Figure 3. Comparison of area under curve (AUC) of a characteristic CH_3 symmetric stretch (2,871 cm^{-1})/CH_2+CH_3 symmetric and aymmetric stretches (3,000-2,812 cm^{-1}) in GBM tumor and control tissue.

Results

A total of 16 raster maps of GBM tumor tissue specimens from 6 patients were obtained and results were compared with 7 maps of control brain tissue specimens from resection margins of two patients, one with craniopharyngioma and the other with astrocytic gliosis. The pathologist of the study confirmed normal brain tissue on histopathological examination of the two control samples (Table I).

Fig. 2A displays a typical IR spectrum of normal brain in comparison with malignant GBM tissue in the spectral region of 3,800-2,600 and 1,900-1,000 cm^{-1}. The spectrum is dominated by the amide I band at ~1,650 cm^{-1} (C=O stretching) and amide II band at ~1,540 cm^{-1} (N-H bending) of the amide groups comprising the peptide linkages of proteins. Peaks at 3,200-2,800 cm^{-1} are mainly due to acyl chain stretchings arising from fatty acids of lipids. The bands in the 1,300-1,000 cm^{-1} region are assigned to symmetric and asymmetric stretching intensities of phosphodioxy groups (PO_2) of DNA. When the IR spectra of the GBM tumor were compared with control samples (Fig. 2A), the following observations were noted: i) in GBM samples, peak intensities of acyl chain vibrations of fatty acids of lipids that appeared at 2,925 and 2,852 cm^{-1} were significantly reduced, while intensities of peaks at 2,957 and 2,871 cm^{-1} showed considerable enhancement. Compared to lipid acyl chain vibrations (3,000-2,800 cm^{-1}), the amide I and II bands (1,719-1,476 cm^{-1}) representing protein were quite intense in GBM tumor indicating that there

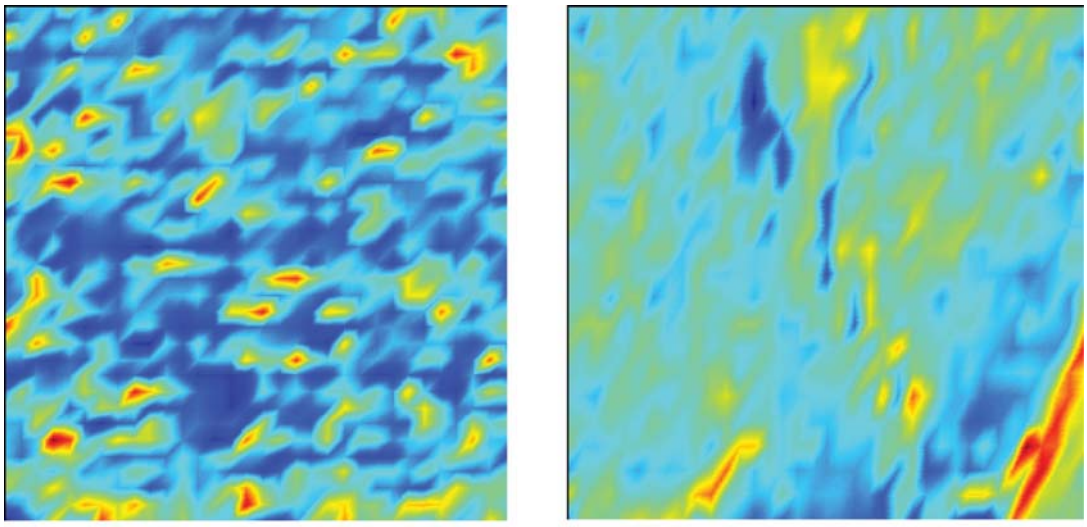

4A 4B

Figure 4. Spectromicroscopic infrared mapping of tissue sections. False color codes represent varying tissue composition. A, Control, specimen displays four different clusters of spectra representing different tissue components. Blue and green pixels represent lipid and protein respectively; yellow and red pixels indicate nucleic acid components. B, GBM, specimen displays marked reduction in lipid component.

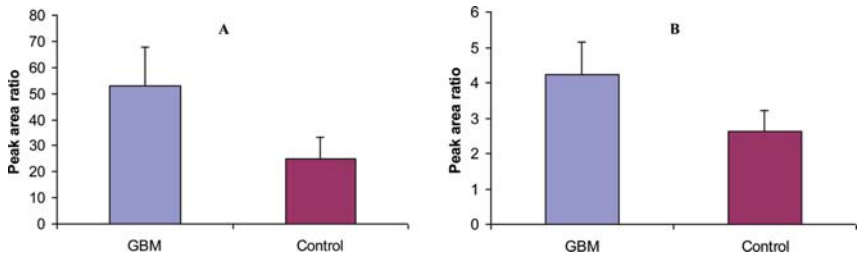

Figure 5. A, Comparison of area under curve (AUC) of amide I+II (1,719-1,476 cm^{-1})/CH_2 symmetric stretch (2,852 cm^{-1}) in GBM tumor and control tissue; B, Comparison of area under curve (AUC) of amide I+II (1,719-1,476 cm^{-1})/CH_2+CH_3 symmetric and asymmetric stretches (3,000-2,812 cm^{-1}) of GBM and control tissue.

is an appreciable reduction of total lipid content compared to total protein content in GBM tumors, ii) the intensities of peaks at ~3,053 cm^{-1} showed noticeable enhancement while peaks at 1,740 cm^{-1} (C=O stretching of lipid ester), ~1,457 cm^{-1} (acyl deformation mode of peptide side chain), ~1,397 cm^{-1} (COO^- amino acid side chain), 1,245 cm^{-1} (PO_2 of DNA) were reduced in GBM samples compared with control, and iii) peaks at 1,397 and 1,245 cm^{-1} in GBM tumor displayed noticeable shifts compared to control while the peak positions of CH_2 and CH_3 stretchings of lipid, and amide I and II peaks remain unaltered.

The CH_3 and CH_2 stretching intensities of lipid in normal brain and malignant GBM tissue appeared in the spectral range of 3,100-2,600 cm^{-1}, and are depicted in Fig. 2B. The bands at 2,925 and 2,852 cm^{-1} arise from symmetric CH_2 stretching modes while the bands at 2,957 and 2,871 cm^{-1} result from asymmetric CH_3 stretching modes of methyl groups of membrane lipid. The asymmetric CH_3 stretching of cholesterol appears at ~ 2,957 cm^{-1} (22). Since the characteristic spectral bands (1,466, 1,376 and 1,365 cm^{-1}) of cholesterol (22) are absent in the tumor tissue, it is possible that the CH_3 asymmetric stretching intensity of vibrations at 2,957 cm^{-1} is due to phospholipids, not to cholesterol. Of interest, intensities of CH_3 asymmetric and symmetric stretches at 2,957 and 2,871 cm^{-1} respectively, show significant enhancement in GBM tumor tissue, compared to normal tissue. This observation was further confirmed by comparing the peak area ratio of the CH_3 asymmetric stretching (2,871 cm^{-1}), representing a particular lipid, with the total peak area contributed by CH_3 and CH_2 symmetric and asymmetric stretching intensities (3,700-2,800 cm^{-1}) of total lipid content. The results in Fig. 3 indicate that there is a significant increase ($p<0.01$) in the peak area of the IR band at 2,871 cm^{-1} in GBM tumors compared to normal tissue. Therefore it is apparent that a particular lipid level has increased in GBM tumors compared to normal tissue, although the total lipid content is found to be drastically reduced compared to protein level (Fig. 5B).

The coloured cluster map representing control tissue (Fig. 4A) clearly reflects four groupings of chemical moieties in normal brain tissue, including lipids, proteins, and nucleic acids. Blue pixels indicating lipid predominate; green and red pixel clusters indicate protein and DNA, respectively. By contrast, in a GBM tumor sample (Fig. 4B), lipid content is reduced drastically while protein content comprises the major portion of the map. To appreciate the change in the lipid content

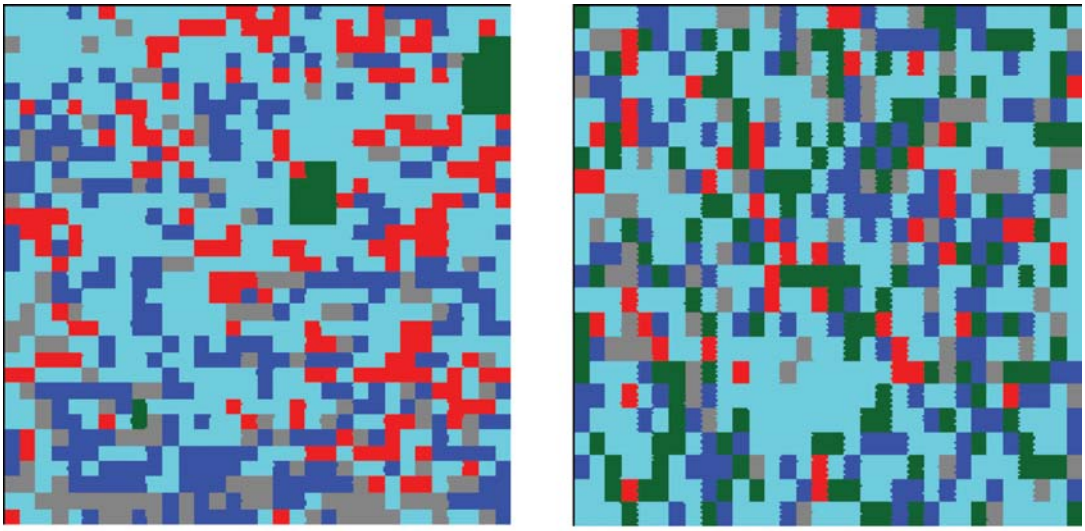

6A 6B

Figure 6. Hierarchial (HCA) cluster analysis of (A) control specimen and (B) GBM tumor specimen. HCA false color image of 5 clusters displaying diversity in tissue composition of tumor tissue compared to control.

in tumor tissue with respect to protein level, the peak areas of amide bands (1,719-1,476 cm^{-1}) representing proteins and peak areas of CH_2 and CH_3 bands (1,719-1,476 cm^{-1}) representing lipids were compared and presented in Fig. 5. Fig. 5A compares the protein/lipid ratios as measured by the peak areas of amide I and II bands in relation to the peak area of CH_2 symmetric stretching band representing lipid, whereas Fig. 5B compares the ratios of peak area of total protein and total lipid content. In both cases, considerable increase in protein to lipid ratio ($p<0.001$) in GBM tumors compared to normal tissue was observed. As a result of the lipid content in GBM tumors being significantly reduced, the total protein to lipid ratio increased 2-fold in GBM compared to normal tissue (Fig. 5B).

Data obtained from spectral comparisons of tumor and control samples graphically display spatial distribution of cluster groups representing different tissue components. Fig. 6 demonstrates false color images displaying the spatial distribution of clusters from our experiments. Five clusters were considered for both control and tumor tissues. Each cluster was assigned a false color code for comparison purposes. The images in Fig. 6A and B, representing control and GBM specimens respectively, clearly differentiate between the spatial distribution of the various clusters identified by the hierarchical cluster analysis (HCA) algorithm (Ward's algorithm). In GBM tumor samples, the cluster representing red pixels, most likely lipid, has been significantly reduced, while clusters identified by green pixels predominate, compared to control sample. These false color cluster images demonstrate the sensitivity of these HCA method techniques in displaying subtle differences not obvious on visual inspection alone.

Discussion

With the ever-increasing array of immunohistochemical and molecular biology techniques for probing GBM tissues, it is becoming apparent that this tumor is heterogeneous in both its histological and molecular structure makeup, when comparing pediatric, young adult, and older adult populations. Increasingly, newer variants of 'classical' GBM including giant cell, small cell, epitheloid, rhabdoid, and those containing PAS and trichrome stain positive intracellular inclusions, are being reported (22,23). These evolutionary changes in the histopathological manifestations of GBM are reflected in the 2007 revision of the original 2002 WHO classifications of tumors of the central nervous system, where newer GBM variants such as GBM with oligodendroglioma component have been recognised (4,5). Therefore, a more precise diagnostic tool is required to capture the molecular biochemical changes at the time of tumor biopsy or resection.

FTIR spectromicroscopy is a more recent investigative technique that is finding ever increasing applications in subcellular recognition of human malignancies (11,24). It has the ability to determine both the functional and quantitative components of lipids, proteins, and nucleic acids, as well as to discriminate between normal, transition interfaces, tumor, and necrotic tissues within and around tumor (25). The resolution of FTIR spectro-imaging approaches the cellular level. It is reported to be reliable in determining distribution of basic biomolecular tissue components, as well as information on molecular secondary protein structure and fatty acyl chain peroxidation level (14). Its ability to function as a biomolecular probe for individual cells *in vitro* without causing toxic or detectable biochemical changes in them allows it to be used as an effective probe at the submicroscopic level (26). This gives credibility to the use of FTIR IR spectroscopy as a new molecular histopathology tool.

Individual biological cells range from 5-30 microns in diameter, too small for probing by conventional IR sources. Synchrotron radiation FTIR is able to overcome this limitation because of its intense brightness that provides a higher signal/noise ratio at the highest spatial resolution (27), thereby permitting intracellular imaging of molecular chemical structure and, compared to globar IR light sources (28), provides greater spectroscopic detail that could serve as a more refined

diagnostic tool (29) for a spectrum of malignant brain tumors, both in terms of differentiating tumor types as well as assessing the degree of anaplasia.

In conclusion, this study demonstrates that there is a significant decrease in the total lipid content compared to protein level in GBM tumor, compared with normal brain tissue. It also identifies a number of significant differences in the mid-IR spectral patterns of GBM tumors compared to normal brain tissue. These differences could serve as diagnostic molecular spectral 'signatures' in identifying residual GBM within tumor resection margins. Further studies with larger number of patients are in progress for precise identification of a molecular signature unique to GBM.

Acknowledgements

This study was funded by a peer reviewed grant from the Saskatchewan Cancer Agency. The research work was conducted at Canadian Light Source, which is supported by NSERC, NRC, CIHR, and the University of Saskatchewan. We thank Shannon Klassen, A.R.T., Department of Pathology, Saskatoon Health Region, for preparation of cryostat tissue sections, and Tor Pedersen, Science Associate, CLS, for his willing assistance at the O1-B1-1 mid-IR beamline.

References

1. Rosenthal MA, Drummond KJ, Dally M, *et al*: Management of glioma in Victoria (1998-2000): retrospective cohort study. Med J Aust 184: 270-273, 2006.
2. Mason WP, Maestro RD, Eisenstat D, *et al*: Canadian recommendations for the treatment of glioblastoma multiforme. Curr Oncol 14: 110-117, 2007.
3. Jeon HJ, Kong DS, Park KB, *et al*: Clinical outcome of concomitant chemoradiotherapy followed by adjuvant temozolomide therapy for glioblastomas: Single-center experience. Clin Neurol Neurosurg 111: 679-682, 2009.
4. Kleihues P, Louis DN, Scheithauer BW, Rorke LB, Reifenberger G, Burger PC and Cavenee WK: The WHO classification of tumors of the nervous system. J Neuropathol Exp Neurol 61: 215-225, 2002.
5. Louis DN, Ohgaki H, Weistler OD, *et al*: The 2007 WHO classification of tumors of the central nervous system. Acta Neuropathol 114: 97-109, 2007.
6. Hassler M, Seidl S, Fazeny-Doerner B, Preusser M, Hainfellner J, Rössler K, Prayer D and Marosi C: Diversity of cytogenetic and pathohistologic profiles in glioblastoma. Cancer Genet Cytogenet 166: 46-55, 2006.
7. Yoshii Y, Moritake T, Yamamoto T, Takano S, Tsuboi K, Hyodo A, Nose T and Satou M: Correlation of histopathological factor of brain tumor and high thallium-201 uptake in single photon emission computed tomography. Noshuyo Byori 13: 61-65, 1996.
8. Oh D and Prayson RA: Evaluation of epithelial and keratin markers in glioblastoma multiforme: an immunohistochemical study. Arch Pathol Lab Med 123: 917-920, 1999.
9. Latza U, Niedobitek G, Schwarting R, Nekarda H and Stein H: Ber-EP4: new monoclonal antibody which distinguishes epithelia from mesothelia. J Clin Pathol 43: 213-219, 1990.
10. Marinkovic NS, Huang R, Bromberg P, Sullivan M, Toomey J, Miller LM, Sperber E, Moshe S, Jones KW, Chouparova E, Lappi S, Franzen S and Chance MR: Center for Synchrotron Biosciences' U2B beamline: an international resource for biological infrared spectroscopy. J Synchrotron Radiat 9: 189-197, 2002.
11. Bruni P, Conti C, Giorgini E, Pisani M, Rubini C and Tosi G: Histological and microscopy FT-IR imaging study on the proliferative activity and angiogenesis in head and neck tumours. Faraday Discuss 126: 19-26, 2004.
12. Lee LS, Chi CW, Liu HC, Cheng CL, Li MJ and Lin SY: Assessment of protein conformation in human benign and malignant astrocytomas by reflectance Fourier transforms infrared microspectroscopy. Oncol Res 10: 23-27, 1998.
13. Bhargava R: Towards a practical Fourier transform infrared chemical imaging protocol for cancer histopathology. Anal Bioanal Chem 389: 1155-1169, 2007.
14. Petibois C and Déléris G: Chemical mapping of tumor progression by FT-IR imaging: towards molecular histopathology. Trends Biotechnol 24: 455-462, 2006.
15. Petibois C, Drogat B, Bikfalvi A, Déléris G and Moenner M: Histological mapping of biochemical changes in solid tumors by FT-IR spectral imaging. FEBS Lett 581: 5469-5474, 2007.
16. Asgari S, Röhrborn HJ, Engelhorn T and Stolke D: Intraoperative characterization of gliomas by near-infrared spectroscopy: possible association with prognosis. Acta Neurochir 145: 453-460, 2003.
17. Carr GL: Resolution limits for infrared microspectroscopy explored with synchrotron radiation. Review Sci Instruments 72: 1613-1619, 2001.
18. Xie AH, He Q, Miller L, Sclavi B and Chance MR: Low frequency vibrations of amino acid homopolymers observed by synchrotron far-IR absorption spectroscopy: Excited state effects dominate the temperature dependence of the spectra. Biopolymers 49: 591-603, 1999.
19. Miller LM and Dumas P: Chemical imaging of biological tissue with synchrotron infrared light. Biochim Biophys Acta 1758: 846-857, 2006.
20. Ali K, Lu Y, Christensen C, May T, Hyett C, Griebel R, Fourney D, Meguro K, Resch L and Sharma RK: Fourier transform infrared spectromicroscopy and hierarchical cluster analysis of human meningiomas. Int J Mol Med 21: 297-301, 2008.
21. Wood BR, Bambery KR, Evans CJ, Quinn MA and McNaughton D: A three-dimensional multivariate image processing technique for the analysis of FTIR spectroscopic images of multiple tissue sections. BMC Med Imaging 6: 12, 2006.
22. Martinez R, Roggendorf W, Baretton G, Klein R, Toedt G, Lichter P, Schackert G and Joos S: Cytogenetic and molecular genetic analyses of giant cell glioblastoma multiforme reveal distinct profiles in giant cell and non-giant cell subpopulations. Cancer Genet Cytogenet 175: 26-34, 2007.
23. Kleinschmidt-DeMasters BK, Meltesen L, McGavran L and Lillehei KO: Characterizations of gliomas in young adults. Brain Pathol 16: 273-286, 2006.
24. Gazi E, Dwyer J, Lockyer N, Gardner P, Vickerman JC, Miyan J, Hart CA, Brown M, Shanks JH and Clarke N: The combined application of FTIR microspectroscopy and ToF-SIMS imaging in the study of prostate cancer. Faraday Discuss 126: 41-59, 2004.
25. Beljebbar A, Amharref N, Leveques A, Dukic S, Venteo L, Schneider L, Pluot M and Manfait M: Modeling and quantifying biochemical changes in C6 tumor gliomas by Fourier Transform infrared imaging. Anal Chem 80: 8406-8415, 2008.
26. Repnytska OP, Dovbeshko GI, Tryndiak VP, Todorb IM and Kosenkovc DV: Structural organization of nucleic acids from tumour cells. Faraday Discuss 126: 61-76, 2004.
27. Salvado N, Buti S, Tobin MJ, Pantos E, John A, Prag NW and Pradell T: Advantages of the use of SR-FT-IR microspectroscopy: applications to cultural heritage. Anal Chem 77: 3444-3451, 2005.
28. Dumas P, Jamin N, Teillaud JL, Miller LM and Beccard B: Imaging capabilities of synchrotron infrared microspectroscopy. Faraday Discuss 126: 289-302, 2004.
29. Holman HY, Bjornstad KA, McNamara MP, Martin MC, McKinney WR and Blakely EA: Synchrotron infrared spectromicroscopy as a novel bioanalytical microprobe for individual living cells: cytotoxicity considerations. J Biomed Opt 7: 417-424, 2002.